Chapter 5

PHASE STABILITY STUDY OF REFRACTORY HEAs

This chapter deals with the synthesis and phase stability study of two refractory high entropy alloys (RHEAs) using theoretical and experimental methods. The first section (5.1) and the second section (5.2) describe the study of TiVZrMoW and TiVZrYHf RHEAs respectively.

5.1 TiVZrMoW refractory high entropy alloy

This RHEAs were first reported in 2010 by Senkov *et al.* [41,141] in two equiatomic NbMoTaW and VNbMoTaW quaternary and quinary alloys consisting of refractory elements (Mo, Nb, Ta, V, W). Both the alloys exhibited a single-phase BCC structure and showed exceptional strength (~400 MPa) at 1600 °C. The yield strength of both the alloys decreased by 30-40% at 600 °C compared to that at room temperature. Above 600 °C, both alloys were reported to have approximately constant yield strength up to 1000 °C. Further, Senkov et al. [127] synthesized four low-density RHEAs with a density of ~6.5 g cc^{-3}, namely NbTiVZr, $NbTiV_2Zr$, CrNbTiZr and CrNbTiVZr, and reported a single BCC phase exhibiting Vickers microhardness of 3.29 GPa, 2.99 GPa, 4.10 GPa and 4.72 GPa, respectively.

Similar encouraging results were reported by other researchers [142–144] about the high-temperature strength and thermal resistance of the refractory HEAs. The nine refractory elements mostly used in RHEAs are positioned in the IV, V, and VI groups of the periodic table. Some non-refractory elements are also added to enhance the solid solution strengthening by formation of intermetallic compounds. Most of the RHEAs studied so far have BCC crystal structure as well as B2 and/or Laves phases. Generally, it is realized that significant softening occurs during deformation at a temperature above

0.6 T_m (where T_m is the absolute melting temperature of an alloy). To overcome this problem of softening at high temperature, it is worth investigating to increase the overall melting temperature and thermal stability of an alloy. In this context, Senkov and his group have done extensive studies on the RHEAs [126,127,142,145–147].

TiZrHfNbV and TiZrHfNbCr refractory alloys were fabricated using an induction melting route by Fazakas et al. [143]. It is important to note that TiZrHfNbV alloy formed a single BCC phase, whereas TiZrHfNbCr exhibited BCC as the major phase co-existing with a small amount of $NbCr_2$ and $HfCr_2$ cubic (C15) Laves phases. The structural and mechanical properties were reported to remain unchanged up to 900 °C. Senkov et al. [142] also prepared RHEAs containing Al, such as $AlMo_{0.5}NbTa_{0.5}TiZr$ and $Al_{0.4}Hf_{0.6}NbTaTiZr$ alloys, to study the effect of replacing Hf with Mo along with variation in Al content. It has been reported that $AlMo_{0.5}NbTa_{0.5}TiZr$ forms two BCC phases with a yield strength of 2000 MPa and 745 MPa at 25 °C and 1000 °C, respectively. On the other hand, $Al_{0.4}Hf_{0.6}NbTaTiZr$ forms a single BCC phase showing a yield strength of 1841 MPa and 298 MPa at 25 °C and 1000 °C, respectively.

Gorr et al. [148] selected MoWAlCrTi alloy following a thermodynamic assessment. The prediction and experimental results to form a disordered single BCC phase were in agreement. The alloy possessed a Vickers hardness of 800 Hv at room temperature and excellent oxidation resistance at high temperatures. Juan et al. [149] modified the strength at high temperatures while retaining the toughness at room temperature in HfNbTaTiZr. In this alloy, they replaced Nb with Mo, whereas in another case, they added Mo to the HfNbTaTiZr quinary HEAs. In both the alloys, there was an improvement in the mechanical properties. It was demonstrated that HfMoNbTaTiZr has a better combination of plasticity and strength. Han et al. [150] studied the effect of Ti addition on the mechanical properties of the BCC phase formed in NbMoTaW and

VNbMoTaW RHEAs. They reported an increase in yield strength at room and also at high temperatures. Bhandari et al. [151] studied the mechanical and thermodynamic properties of MoNbTaTiW refractory HEAs using the first principles and CALPHAD approaches. The mechanical properties were calculated using a unit cell having 100 randomly distributed atoms over it. It was reported that the calculated and experimental results were in good agreement. Guo et al. [152] improved the high-temperature strength of TiNbMoW alloy by the addition of Si. It appeared that the addition of Si caused the formation of silicide, which enhanced hardness and strength. Most of the RHEAs reported in literature showed the formation of a BCC phase as the primary and major one. It may be because elements from V and VI groups have BCC structures and elements of the IV group exhibit allotropic transformation to BCC at higher temperatures. The second frequently observed phase in the RHEAs is the Laves phases (C14 and C15 type Laves phases) [153,154]. The reason for the evolution of the Laves phase arises from considerable variation in atomic radii ($\frac{r_A}{r_B} \sim 1.22$) of refractory elements satisfying the criteria for the formation of the AB_2 Laves phase. Though the Laves phases in the BCC matrix decrease ductility of the alloy at room temperature, it also increases high-temperature strength and stability.

Mu et al. [144] studied TiVZrMo, TiVZrMoTa, TiVZrNbMoTa, TiVCrZrNbMoTa, and TiVCrZrNbMoTaW alloys and obtained a single-phase BCC solid solution. They employed the *ab-initio* method to estimate formation enthalpy and cohesive energy to study the ability of the above refractory alloys. They calculated the theoretical elastic constant and bulk modulus for all the alloy systems, which exhibit variation in mechanical anisotropy.

A theoretical and experimental investigation of new TiVMoZrW RHEA was carried out in the present study to understand the phase evolution and stability. As this alloy was not studied so far, the aim of the present work was to add W and to study its effect on the evolution of phases and thermal stability. Being a high melting point element, W was expected to enhance the thermal stability of the previously studied TiVZrMo quaternary alloy.

5.1.1. Phase prediction by theoretical models

To predict the phase stability, we have calculated a few parameters as reported by several researchers [21,37,43,48,155]. These consisted of enthalpy of mixing (ΔH_{mix}^{Mied}) (Miedema's method), atomic size mismatch (δ), valence electron concentration (VEC), electronegativity difference, etc. The calculation of enthalpy of mixing for the binary alloy subsystems is shown in **Table 2.1**. It shows that Ti-Zr, Mo-V, V-W, and Mo-W binary systems have good mutual solubility, whereas V-Zr, Mo-Zr, and W-Zr are having a significant negative enthalpy of mixing, indicating the formation of intermetallic phases. Ti-V and Ti-Mo have a small deviation from the ideal conditions that favor forming a solid solution. Using a regular solution model on the binary subsystems, we calculated the enthalpy of mixing ($\Delta H_{mix}^{Mied} \approx$ -5 kJ.mol^{-1}) for quinary equiatomic composition (**Equation 1.13**), as shown in **Table 5.1**. Atomic size mismatch (δ) was calculated (**Equation 1.15**) using the relation proposed by Zhang [38] for establishing a solid solubility relationship for multicomponent systems. They reported that for a solid solution to form, δ should be ≤ 6.6. Choosing VEC over e/a defined by Hume-Rothery was due to the variation of e/a values for transition elements in a different environment. VEC [36] of the multicomponent alloy system (using **Equation 1.16**) is defined as the weighted average of VEC values of each constituent element. It has been shown that a

single-phase FCC solid solution forms for VEC ≥ 8, whereas a single-phase BCC solid solution is expected for VEC ≤ 6.8 [35]. For intermediate values of VEC, a two-phase mixture of FCC and BCC phases is expected.

Table 5.1: Enthalpy of mixing for all the binary subsystems in TiVZrMoW HEA in kJ.mol^{-1}.

i - j	**TiV**	**TiZr**	**TiMo**	**TiW**	**VZr**	**MoV**	**VW**	**MoZr**	**WZr**	**MoW**
ΔH_{mix}^{ij}	-2	0	-4	-6	-3	0	-1	-6	-9	0

A dimensionless term, Ω defined as the ratio of the terms $T_m \Delta S_{mix}$ and magnitude of ΔH_{mix} advocated by Yang and Zhang [48] was also calculated (**Equation 1.17**) to check solid solution formation criteria. This parameter consists of terms that appear in the calculation of Gibbs function ($\Delta G_{mix} = \Delta H_{mix} - T\Delta S_{mix}$) and it measures the competition between enthalpy and entropy terms. The melting temperature of the quinary alloy T_m was calculated by the rule of mixture applied to the melting temperatures of the constituent elements. The solid solution formation tendency increased when the entropy effect increased, i.e., $\Omega \geq 1.1$, and when enthalpy dominated, then the formation of a mixture of phases was favoured. In the present case, Ω is 2.68, more significant than 1.1. Thus Ω parameter calculated here indicates a favourable situation for the formation of a solid solution phase at 1000 °C.

Table 5.2: Phase stability parameters calculated by empirical formulas.

ΔH_{mix} **kJ.mol^{-1}**	ΔS_{mix} **J.mol^{-1}K^{-1}**	δ*100	*VEC*	Ω
-4.98	13.38	7.17	5	2.68

We calculated the binary phase diagrams for the ten binary subsystems that formed on choosing five elements using Thermo-Calc software. Binary alloy subsystems were computed using the SGTE solution database version 5 (SSOL-5). We noticed that Ti-V, Ti-Mo, Ti-W, Ti-Zr, and Mo-W formed a disordered BCC phase. Three of these (Ti-V, Ti-Mo and Ti-W) systems had disordered BCC and HCP structures at room temperature. The two binary systems (Mo-V and V-W) had BCC phase at higher temperatures and a mixture of two ordered B2 phases at room temperature. The remaining three binary systems had a mixture of ordered B2 and C15 type Laves phases at higher temperatures and a combination of disordered HCP and C15 type Laves phases at room temperature. The equilibrium diagram of the chosen quinary alloy system was calculated using Thermo-Calc software. **Figure 5.1** shows that above ~600 °C, only two B2 phases were stable. However, below 600 °C, a multiphase structure was obtained, containing three B2 phases along with two C15 type Laves phases. The compositions of the B2 phases obtained were also calculated using a single point equilibrium temperature at 500 °C and 800 °C, as shown in **Table 5.3** and **Table 5.4**.

The FCC, BCC, and HCP phases were geometrically relaxed to calculate all the constituent elements' equilibrium lattice parameters. The calculated lattice parameters were tabulated in **Table 5.4**. The enthalpy of mixing of binary alloys for all the subsystems and the three crystal systems are given in **Table 5.5**. The enthalpy of mixing for the quinary system was calculated for all three crystal systems using the regular solution model. From **Table 5.5**, one can easily conclude that the BCC phase is more stable, having the lowest enthalpy. As the enthalpy of mixing for the BCC crystal structure is moderately positive, phase separation at lower temperatures could be possible. Thus stable BCC phase may result in a mixture of the BCC phase and some intermetallics. Based on the binary phase diagram, three Laves phases of C15 type may

form. The formation enthalpy of all the three Laves phases (ZrW_2, $ZrMo_2$ and ZrV_2) and the possible ternary Laves phase, i.e., $Zr(Mo, W)_2$ were calculated using DFT. The enthalpy of formation and respective lattice parameters as calculated are tabulated in **Table 5.6**.

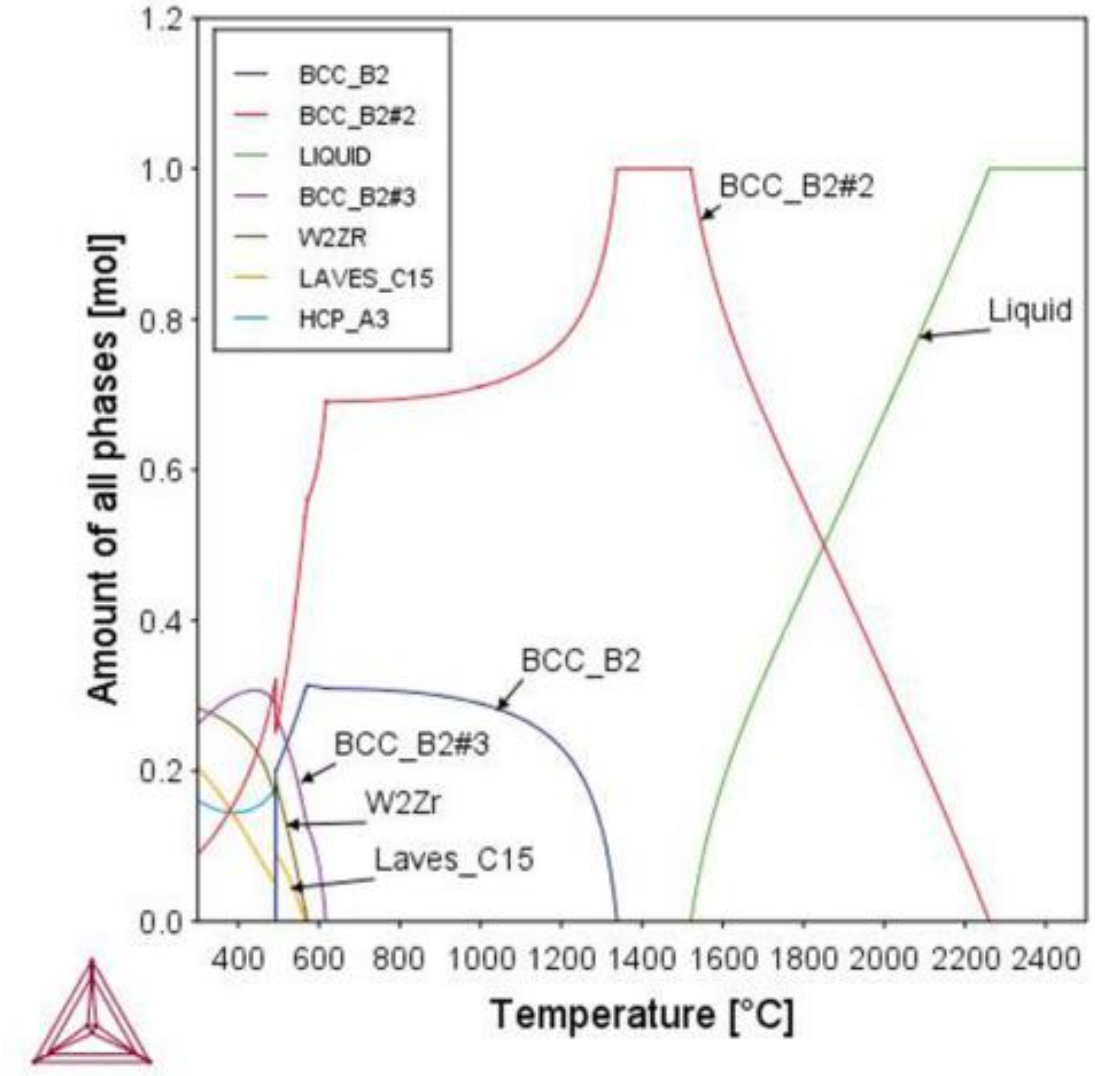

Figure 5.1: Amount of equilibrium phases as a function of temperature. The figure shows two significant phases, bcc1 (BCC_B2#2) and bcc2 (BCC_B2), above 600 °C.

Table 5.3: Composition of all phases formed at 1400 °C, 800 °C, 500 °C and 300 °C in a mole fraction estimated by single point equilibrium calculations.

Temp (°C)	Stable phases	Mole fraction	Ti	V	Zr	Mo	W
1400	**bcc1#B2**	1	0.200	0.200	0.200	0.200	0.200
800	**bcc1#B2**	0.690	0.181	0.242	0.043	0.250	0.283
	bcc2#B2	0.310	0.242	0.104	0.557	0.086	0.011
500	**bcc1#B2**	0.272	0.228	0.087	0.014	0.443	0.228
	bcc2#B2	0.209	0.363	0.085	0.510	0.039	0.003
	bcc3#B2	0.265	0.233	0.598	0.018	0.060	0.090
	$ZrMo_2$	0.083	0.000	0.000	0.333	0.667	0.000
	ZrW_2	0.171	0.000	0.000	0.333	0.000	0.667
300	**bcc1#B2**	0.090	0.261	0.006	0.002	0.691	0.041
	bcc2#B2	0.263	0.210	0.751	0.002	0.009	0.028
	hcp	0.161	0.755	0.231	0.013	0.000	0.000
	$ZrMo_2$	0.204	0.000	0.000	0.333	0.667	0.000
	ZrW_2	0.283	0.000	0.000	0.333	0.000	0.667

Table 5.4: Lattice parameters of constituent elements calculated by DFT are used to predict the lattice parameter of phases formed at 800 °C.

Elements	BCC a (Å)	FCC a (Å)	HCP a; c/a (Å)	Lattice parameter bcc 2 (800°C)	Lattice parameter bcc1 (800°C)
Ti	3.24	4.11	2.94; 1.58	3.42 Å	3.15 Å
V	3.02	3.81	2.95; 1.63		
Zr	3.57	4.52	3.23; 1.59		
Mo	3.15	4.01	2.78; 1.78		
W	3.16	4.04	2.76; 1.77		

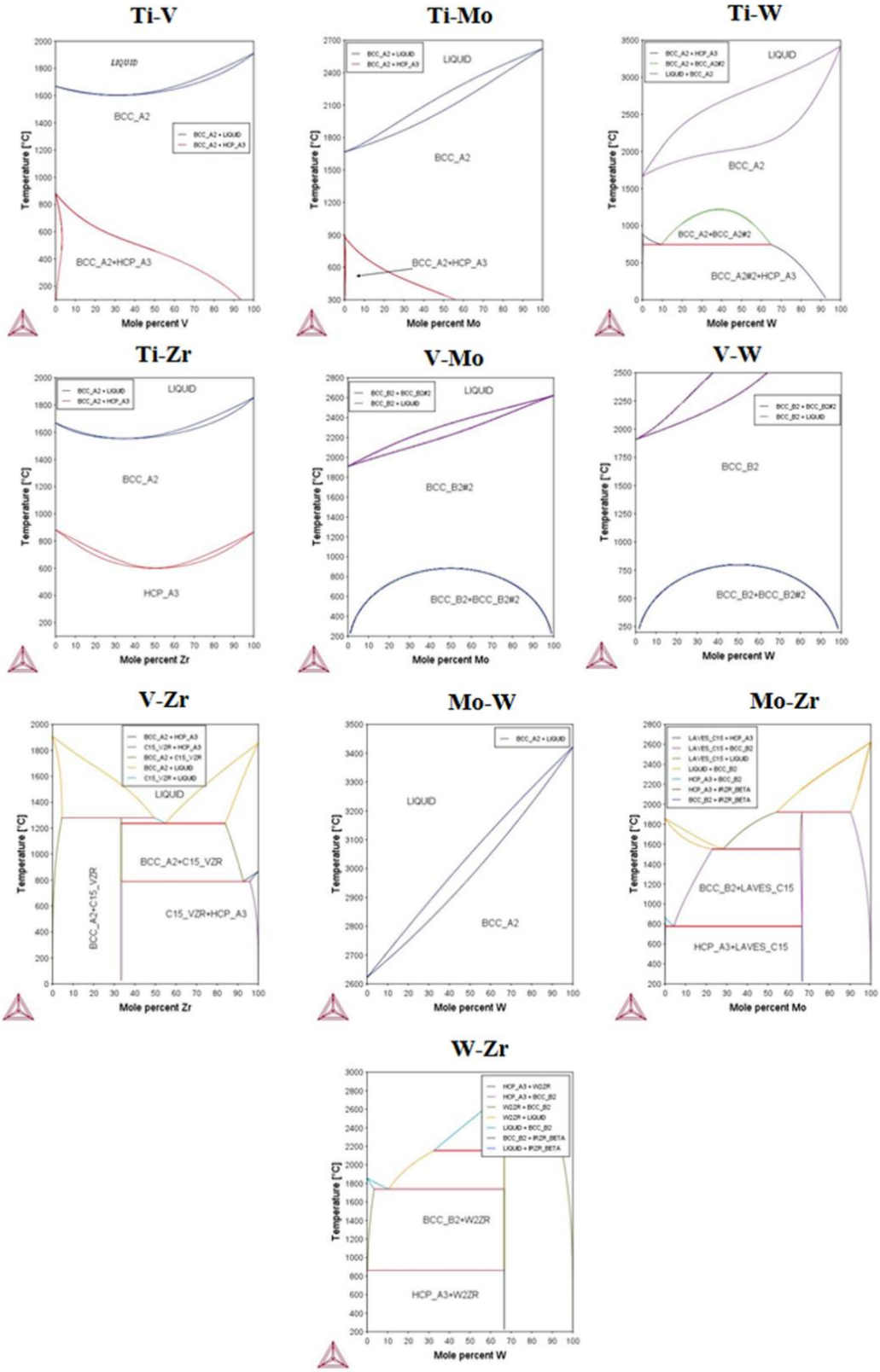

Figure 5.2: Phase diagrams of binary subsystems calculated by Thermo-Calc showing equilibrium phases with varying temperatures.

Table 5.5: Enthalpy of mixing for all binary subsystems in TiVZrMoW HEA using DFT.

Binary subsystems	**BCC** (ΔH_{mix}^{ij} , **kJ.mol^{-1}**)	**FCC** (ΔH_{mix}^{ij} , **kJ.mol^{-1}**)	**HCP** (ΔH_{mix}^{ij} , **kJ.mol^{-1}**)
Ti-V	4.1204	8.6937	5.2904
Ti-Zr	6.9576	6.6868	5.4988
Ti-Mo	-10.0672	-13.9686	-9.7944
Ti-W	-6.0206	-9.3189	7.8289
V-Zr	18.2817	23.3587	6.8755
V-Mo	-6.3110	-6.0551	26.9672
V-W	-5.1493	-10.8581	-19.8247
Zr-Mo	7.6057	16.1862	-10.0245
Zr-W	13.8955	17.9141	-5.8024
Mo-W	3.2556	-4.1499	29.1398
ΔH_{mix}^{DFT} **(kJ mol^{-1})**	**4.2509**	**4.5582**	**5.7847**

Table 5.6: Enthalpy of formation of possible intermetallic phases based on binary phase diagrams in the TiVZrMoW HEA, calculated using DFT.

Intermetallic phases	**ZrV_2**	**$ZrMo_2$**	**ZrW_2**	**$Zr(Mo,W)_2$**
Enthalpy of formation (kJ.mol^{-1})	-10.77	-40.47	-45.03	-42.49
Lattice Parameter (Å)	7.38	7.56	7.62	7.59

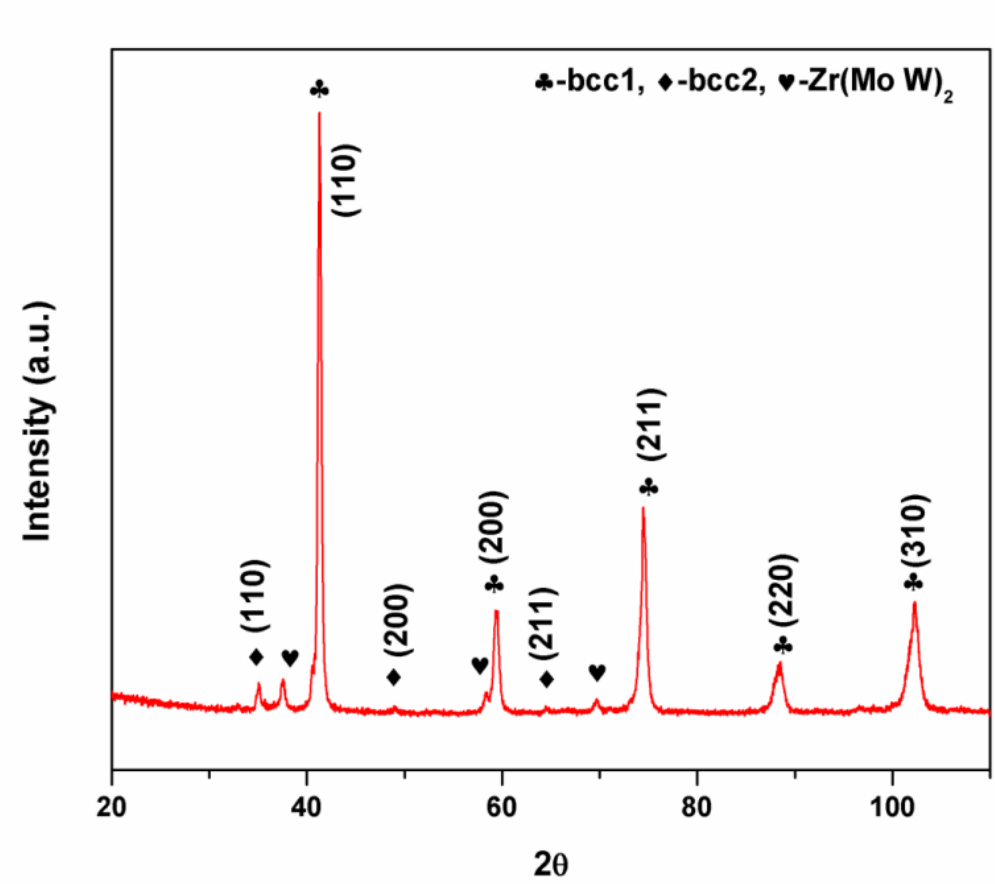

Figure 5.3: Phases evolved in the as-cast TiVZrMoW refractory high entropy alloy.

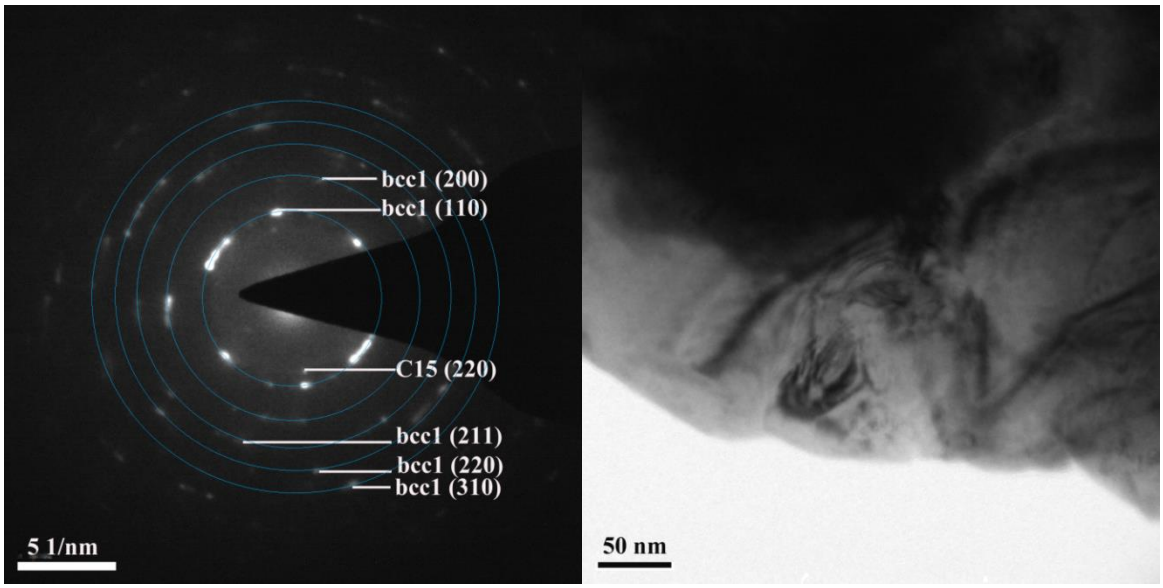

Figure 5.4: (a) Selected area diffraction (SADP) of powdered as-cast TiVZrMoW with an overlapped ring. (b) bright field image corresponding to SADP in figure 5.4(a).

5.1.2. Phase evolution and microstructure in the as-cast and annealed sample

The XRD analysis of as-cast TiVZrMoW was shown in **Figure 5.3**. The indexing of the diffraction peaks showed the presence of two BCC phases, i.e., bcc1 (a = 3.17 ± 0.02 Å) and bcc2 (a2 = 3.65 ± 0.02 Å). Few peaks of Laves phases (C15 type) having a lattice parameter of a = 7.58 ± 0.02 Å were also observed. The present quinary alloy had three BCC elements along with two HCP elements. The two HCP elements had an allotropic transformation to BCC at high temperatures. Thus the formation of the BCC phase in the present alloy was likely to be more favourable.

The TEM analysis of the as-cast powdered sample of TiVZrMoW was shown in **Figure 5.4**. Indexing of the spot pattern shows bcc1 phase (a = 3.17 ± 0.02 Å) along with weak diffraction spot corresponding to Laves phase (C15) (a = 7.58 ± 0.02 Å). The morphology of the grains obtained from SEM was shown in **Figure 5.5.** We could see randomly oriented dendritic type grains from the figure, evolved due to the fast cooling rate obtained in a water-cooled copper mould used in vacuum arc melting. The grain boundaries might have a second phase that got etched during etching. STEM-EDS mapping of the as-cast powdered sample was shown in **Figure 5.6**. The grey patches in the HAADF image were rich in Zr and Ti, while bright areas were more affluent in Mo and W. The element V is distributed in both Zr rich and Mo-W affluent regions.

The thermal stability of the as-cast alloy was studied using DSC, as shown in **Figure 5.7**. Results showed two endothermic peaks in the temperature range 375 °C – 630 °C. The endothermic peak obtained represented the solid-solid transformation. As this alloy had some degree of phase separation tendency, diffusion-assisted transformation occurred, showing shallow peaks in the graph. It was observed that above 620 °C, the alloy was stable up to 1000 °C, as there were no other peaks identified in this temperature range.

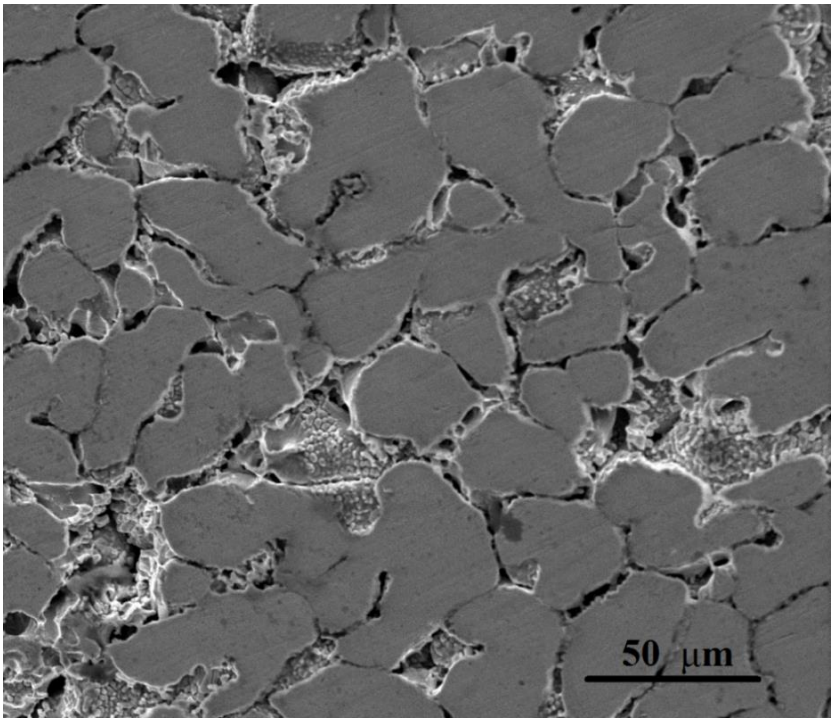

Figure 5.5: SEM micrograph of as-cast TiVZrMoW RHEA showing dendritic type microstructure.

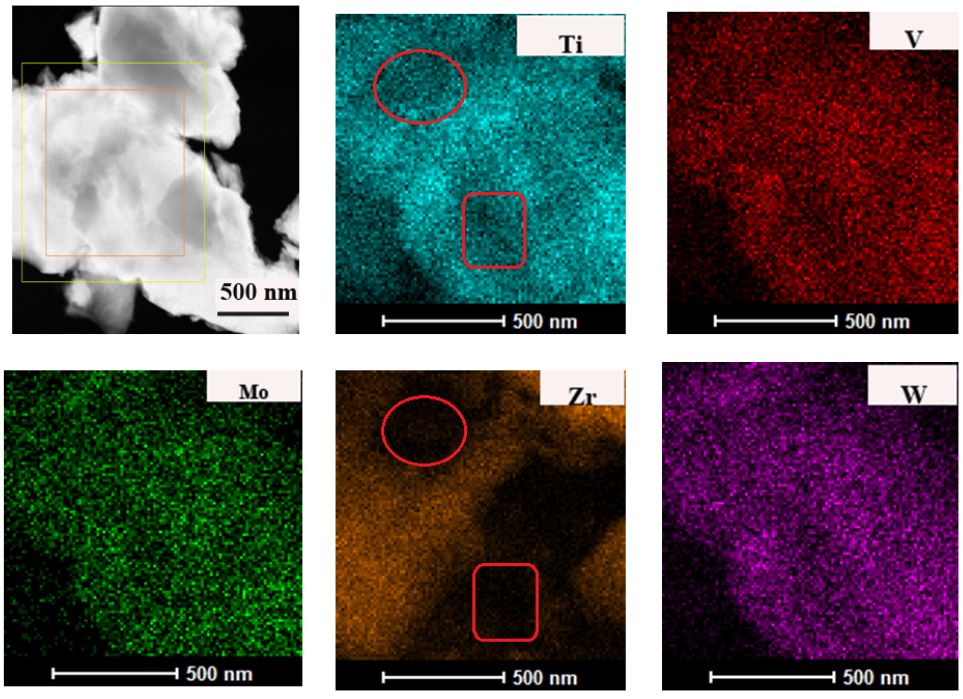

Figure 5.6: STEM-EDS analysis of the as-cast powdered sample. The oval and rectangular areas marked on Ti and Zr are show lean regions in the elemental mapping.

XRD pattern of the annealed sample was shown in **Figure 5.8**. We could see from the diffraction peaks that there was an evolution of (100) superlattice peak corresponding to the ordered B2 phases. The Laves phase was found to be stable, and the amount of phase increased significantly in the annealed sample. Interestingly, peaks corresponding to the bcc2 phase were broader and had shoulder peaks signifying that ordered and disordered forms of bcc2 phases were present. It may be noted that this phase was enriched in Zr, and the transformation at this temperature perhaps was not completed. The SEM micrograph of the annealed sample shown in **Figure 5.9** showed the grain size increased during heat treatment. The separation between the phase particles increased significantly. The elemental mapping of the annealed sample by SEM-EDS showed a uniform distribution of all constituent elements within the selected area (**Figure 5.10**). The spot analysis on the primary phase after scanning showed the even distribution of Mo, W, and V (**Figure 5.11**). The minor variation in chemical composition from the estimated composition might be due to sluggish diffusion of the constituent elements.

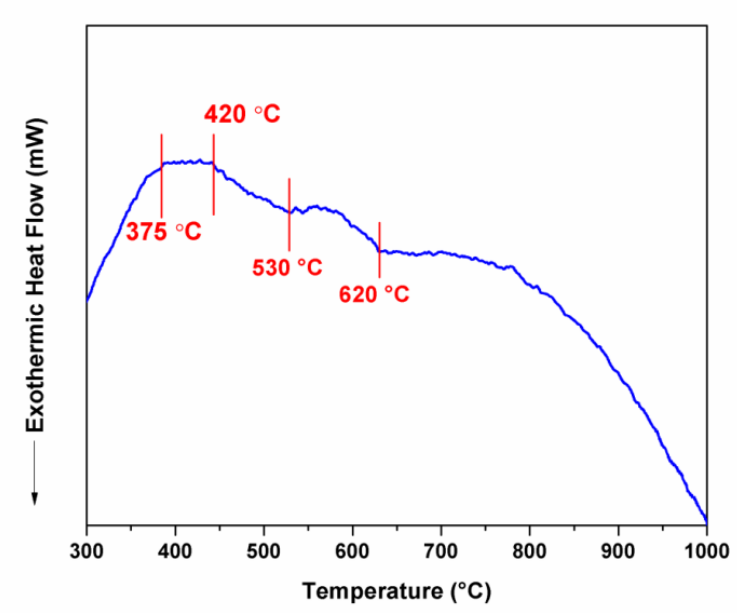

Figure 5.7: DSC thermogram of as-cast powdered TiVZrMoW HEA showing solid-solid transition (endothermic peak).

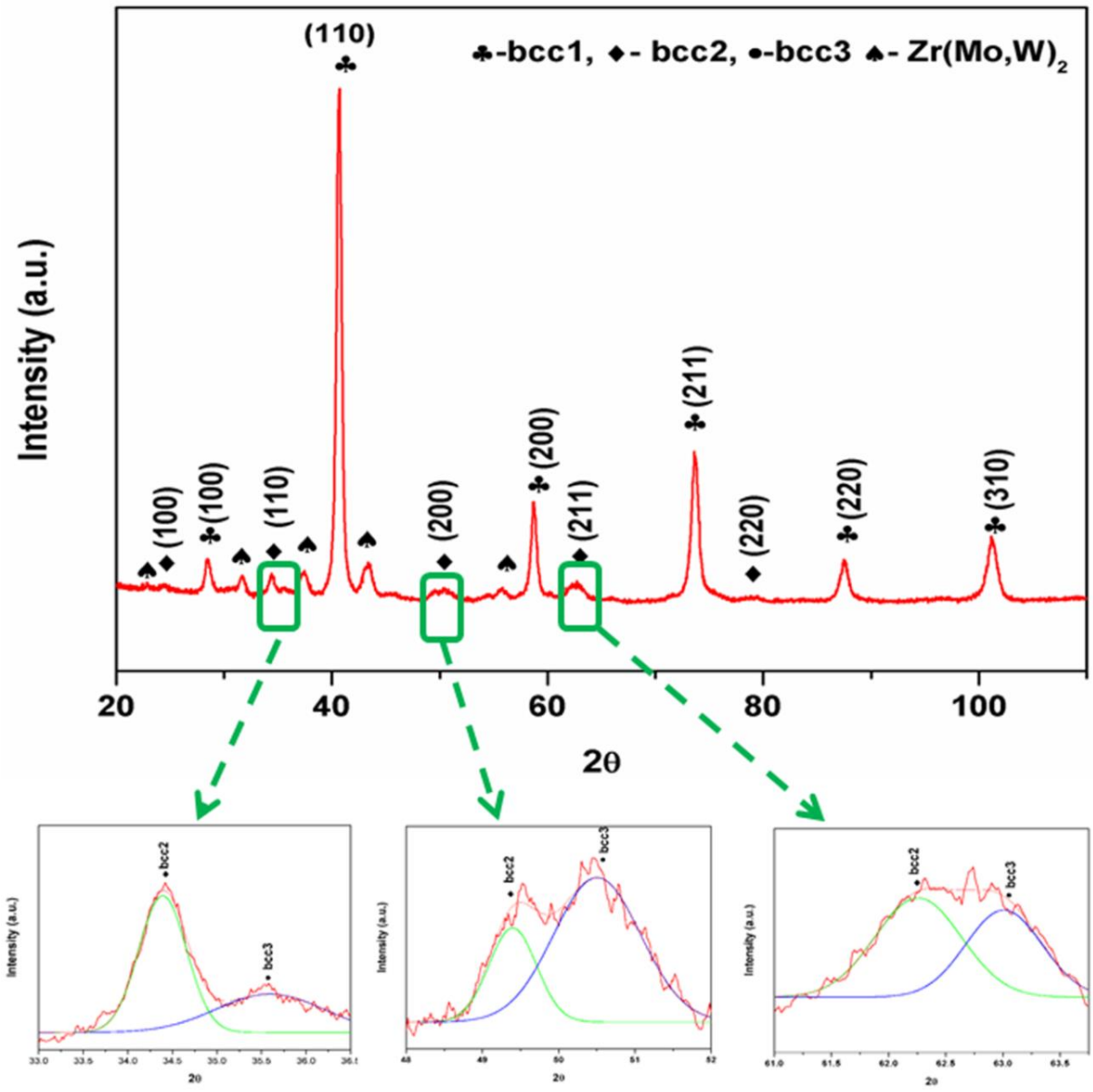

Figure 5.8: XRD analysis of the annealed vacuum-sealed sample at 900 °C for 7 h. We have indexed two ordered B2 (bcc1 and bcc2) along with one disordered BCC phase, as shown in the pop-up window shown adjacent to the bcc2 phase from the diffraction.

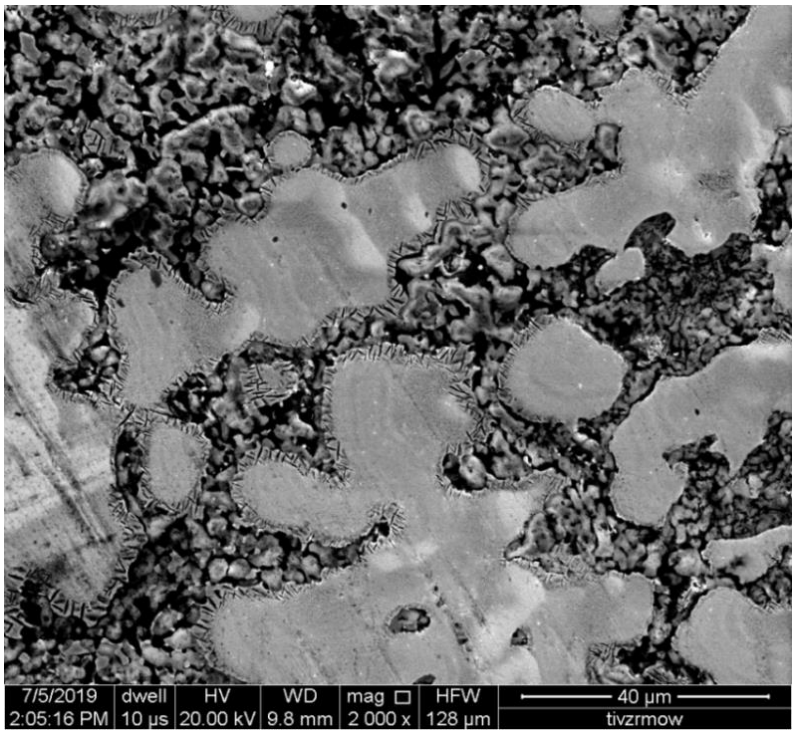

Figure 5.9: SEM micrograph of the annealed TiVZrMoW RHEA at 900 °C for 7 h.

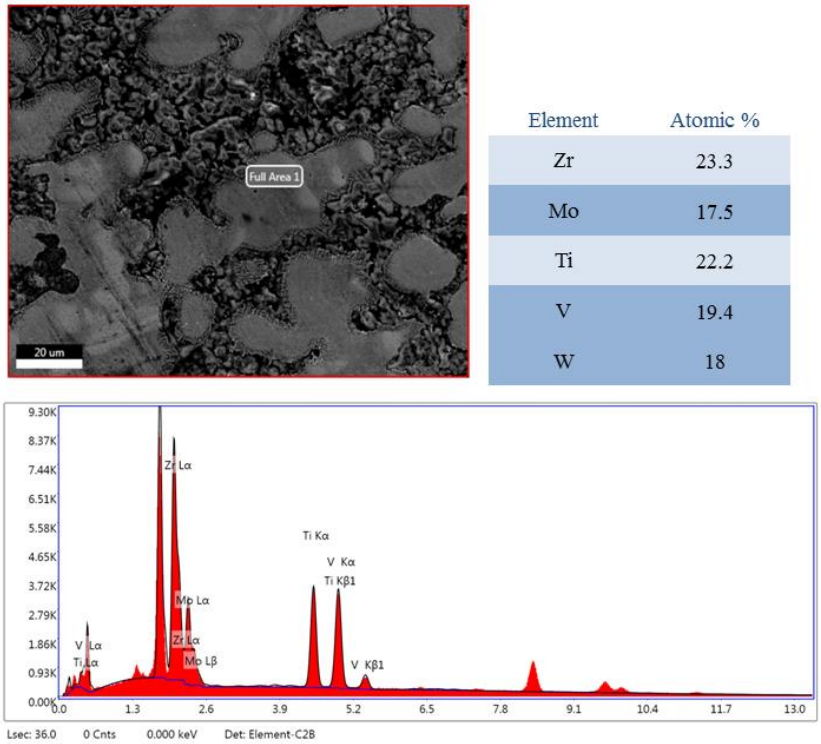

Element	Atomic %
Zr	23.3
Mo	17.5
Ti	22.2
V	19.4
W	18

Figure 5.10: SEM-EDS mapping of the full captured area showing the composition close to the equiatomic composition.

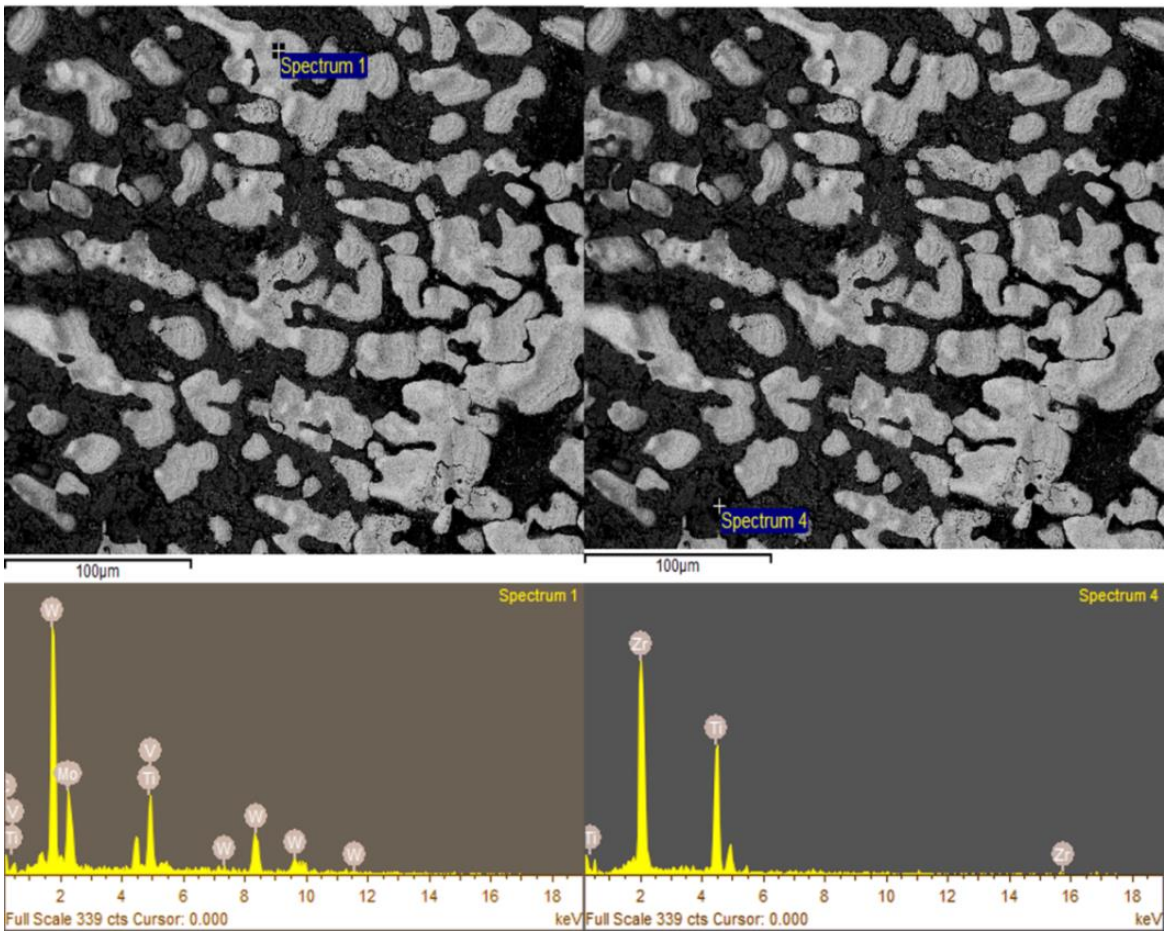

Figure 5.11: SEM-EDS analysis of a micron area (a) taken on the grey phase (W, Mo and V rich). (b) Taken from the dark phase (Ti and Zr rich) of annealed TiVZrMoW RHEA

5.1.3 Discussion

We did some parametric calculations based on extension of Hume-Rothery rules for multicomponent alloys as advocated in literature to predict the phases and their stability. The enthalpies of binary subsystems were calculated using Miedema's model [45] (using **Equation 1.13**) and tabulated in **Table 5.1**. The binary enthalpy values had a significant role in predicting how an element would interact with the other constituent elements in a multicomponent alloy. From **Table 5.1,** it was expected that Ti-Zr and Mo-W could have good mutual solubility, whereas V-Zr, Mo-Zr and W-Zr having significant negative enthalpy could have a tendency to form intermetallics. However, having small

negative enthalpy values for Ti-V, Ti-Mo and Ti-W binary subsystems could be easily stabilized by the configurational entropy of mixing. It seemed that atomic size mismatch acted as a crucial parameter in deciding the phase stability. According to Zhang et al. [47], the calculated parameters (enthalpy of mixing, VEC and size mismatch) must lie within a specified range for solid solution formation. The criteria for single-phase formation were stated to be (i) $\Delta S_{config} \geq 13.38\,\mathrm{Jmol^{-1}K^{-1}}$, (ii) $-10 \leq \Delta H_{mix} \leq 5\,\mathrm{kJmol^{-1}K^{-1}}$, (iii) $\delta \leq 6.6\%$. Guo and Liu [36] suggested additional criteria based on VEC for the formation of a single-phase solid solution. According to this criterion, $VEC > 8$, $8 \geq VEC \geq 6.87$ and VEC < 6.87 could lead to the formation of FCC structure, a mixture of FCC and BCC structure, and BCC structure alone, respectively. The enthalpy of mixing and VEC values in the present investigation were indicating towards the formation of BCC solid solution phase. At the same time, the atomic size mismatch was higher than that of the ideal value, implying that this factor could de-stabilize the lattice to form multi-phase structures. Accordingly, one can understand the rationale for the evolution of multiphase in the present investigation.

The phase diagrams of binary subsystems may explain the phases that were evolved in the as-cast alloy. The binary systems Ti-Zr, and Mo-W have an enthalpy of formation zero, indicating good mutual solubility. The binary phase diagram shown in **Figure 5.2** confirms good mutual solubility over the entire composition regime in the Mo-W and Ti-Zr systems. The stable phases at low and high temperatures based on the phase diagram calculation can be summarized below.

Binary systems	**Equilibrium phases at room temperature**	**Equilibrium phases above 1000 °C**
Ti-V	BCC_A2 + HCP_A3	BCC_A2
Ti-Mo	BCC_A2 + HCP_A3	BCC_A2

Ti-W	BCC_A2 + HCP_A3	BCC_A2
Ti-Zr	HCP_A3	BCC_A2
V-Mo	BCC_B2 +BCC_B2#2	BCC_B2
V-W	BCC_B2 +BCC_B2#2	BCC_B2
Mo-W	BCC_A2	BCC_A2
V-Zr	C15_ZrV_2 + HCP_A3	BCC_A2 + C15_ZrV_2
Mo-Zr	C15_$ZrMo_2$ + HCP_A3	BCC_B2 + C15_$ZrMo_2$
W-Zr	C15_ZrW_2 + HCP_A3	BCC_B2 + C15_ZrW_2

Considering the above facts and melting point of elements from **Table 2.1**, it may be inferred that W rich liquid would start solidifying first, followed by Mo and other elements. As both components have good mutual solubility, they would form a disordered BCC (BCC_A2) phase. The next solidifying element would be V, Zr and Ti dissolving in BCC_A2 at the higher temperature. Thus a quinary disordered BCC solid solution formed at higher temperatures. A multicomponent alloy was expected to form a single-phase disordered solid solution at high temperature because of the high entropy effect. However, as the temperature decreased, the thermal entropy effect of the quinary system decreased, resulting in the rejection of elements from the disordered phase. With falling temperature, Zr being immiscible with V, Mo, W was getting rejected first, followed by Ti. Thus, Ti-Zr having good mutual solubility among them compared to that of V, Mo and W, formed another disordered solid solution (bcc2). Due to the presence of Laves phases at high and low temperatures in the three binary systems (Ti-V, Ti-Mo and Ti-W), the evolution of cubic Laves phases in the present alloy appeared to be a distinct possibility. The three binary systems (V-Zr, Mo-Zr and W-Zr) formed a mixture of disordered HCP and an ordered intermetallic phase with AB_2 stoichiometry. In each case,

the AB_2 type cubic Laves phase (C15) could form. Considerable variation in the atomic radius of Zr compared to V, Mo and W also supported the formation of Laves phases in the present quinary alloy. Due to the rapid cooling rate during the processing of as-cast alloy, the precipitation of the Laves phases might not have been completed, as the amount of Laves phase in the annealed sample was found to have increased.

The XRD result of the annealed sample can be understood with the help of the DFT (**Table 5.5**) and equilibrium phase diagram (**Figure 5.2**). The DFT calculation showed the enthalpy of mixing for the BCC phase to be 4.25 $kJ.mol^{-1}$. The positive deviation in the chosen alloy showed phase separation tendency. The miscibility gap for the enthalpy value might exist up to ~300 K (calculated using the regular solution model). Thus a multi-phase microstructure at room temperature could be expected.

Similarly, after analyzing the equilibrium phase diagram of TiVZrMoW (**Figure 5.2**), the multiple phases could be seen at low temperatures. The reactions and the transformation temperatures of phases from the equilibrium diagram (calculated using the CALPHAD approach) were summarized below

Reaction	Temperature (°C)
Liquid → BCC_B2#2 (bcc1)	2260
BCC_B2#2 → BCC_B2 (bcc2)	1340
BCC_B2 + BCC_B2#2 → BCC_B2#3	620
BCC_B2 + BCC_B2#2 → $ZrMo_2$+ZrW_2	580
BCC_B2 + BCC_B2#2 → HCP_A3	500

From the above description, it was clear that the ordered B2 structure was stable in the equilibrium diagram. The composition of all the phases formed in the equilibrium diagram was tabulated in **Table 5.3**. From the table, it can be noted that the primary phase was rich in W, Mo and V while the minor B2 phase was rich in Ti and Zr. This was

validated experimentally from the XRD analysis of diffraction peaks. Both the equilibrium phase diagram and XRD peaks showed the presence of some amount of cubic Laves phase. Seven binary systems formed disordered HCP at low temperature, indicating the possibility of HCP phase formation at low temperature. But due to fast cooling in the copper mould (vacuum arc furnace) and slow diffusivity of the elements in this alloy, the formation of the HCP phase could not have occurred and accordingly it was not observed in XRD pattern.

Thus, in the as-cast and annealed sample, diffraction peaks also confirm Mo-W and Ti-Zr rich BCC phases (**Figures 5.3 and 5.8**). Due to high negative enthalpy values, both Mo-Zr and W-Zr had tendency to form intermetallic phases, as Mo and W has good mutual solubility, the ternary intermetallic phase might have formed Zr(Mo, $W)_2$ as it matched closely with XRD peaks. The two binary Laves phases had very close lattice parameters (7.58 Å and 7.62 Å). The formation enthalpy of the ZrV_2, $ZrMo_2$, ZrW_2 and Zr(Mo, W) were calculated using DFT and were tabulated in **Table 5.6**. Considering the formation enthalpy of intermetallics, it showed the tendency to form ZrW_2 having the smallest enthalpy value. However, the enthalpy of formation of $ZrMo_2$ and Zr(Mo, $W)_2$ were close to ZrW_2. Thus, the formation of ZrW_2, Zr(Mo, $W)_2$ and $ZrMo_2$ decreased the order of probability of appearance. Comparing the lattice parameter of the above three intermetallic phases as calculated using DFT and the one obtained from the XRD analysis, the formation of ternary Zr(Mo, $W)_2$ Laves phase in the present alloy was justified.

We have used the composition of the phases obtained using a single point equilibrium calculation to predict the lattice parameter of two BCC phases (**Table 5.4**). The lattice parameter for all the elements (for BCC, FCC and HCP phase) was calculated using DFT. Using the rule of mixture, the lattice parameter of bcc1 and bcc2 was

estimated to be 3.15 Å and 3.42 Å, respectively. The lattice parameter of bcc1 matches closely with the experimental value (3.17 Å). There is a deviation in the predicted lattice parameter of bcc2. This may be due to the variation of enthalpy and composition of the bcc2 in predicted and as-cast alloys.

The STEM-EDS mapping of the as-cast alloy shows Zr and Ti-rich region and W, Mo and V rich region. The SEM micrograph of the as-cast sample, as shown in **Figure 5.6,** showed a dendritic type of structure. Mu et al. [144] reported that high melting temperature elements were contained in dendrites and lower melting point elements segregated in the inter-dendritic regions in such microstructures. Thus, the primary phase may contain Mo (M.P. 2617 °C) and W (M.P. 3410 °C) as the major constituent element, along with small amounts of other elements. However, the dark inter-dendritic region (bcc2) phase may consist of V (M.P. 1890 °C), Zr (M.P. 1852 °C) and Ti (M.P. 1660 °C) rich phases (bcc2). SEM micrograph of the annealed sample showed bright precipitate and a mixture of the dark and bright matrix. From the composition analysis it was found that the bright phase was rich in W, Mo and V, while the dark areas in the matrix were Ti and Zr-rich, as shown by SEM-EDS mapping (**Figure 5.11**). The SEM-EDS of the full captured area showed a uniform distribution of all constituent elements (**Figure 5.10**). The three phases were distinctly identified in the as-cast and annealed sample, and it also supported the prediction of models adopted in the present investigation.

5.2 TiVZrYHf refractory high entropy alloy

The density functional theory (DFT) was used to solve complex many-particle Schrodinger equation; which could act as a powerful tool for predicting the formation of phases (e.g., BCC, FCC, and HCP) and their stability under different conditions. The stability of these various phases was determined by the relative energy of the individual atoms' specific arrangement on a given lattice type and concentration. The disordered

solid solution cell was designed mainly by Coherent Potential Approximation (CPA) [96], Special Quasirandom Structure (SQS) [97], and Cluster Expansion method [98]. The cluster expansion method, [98,156–158], was used for nearly 30 years to study the mixing of two (or more) atoms for a given lattice symmetry by changing the concentration of different atom types computing the relative energy by DFT calculation. Thus we focused on the total energy (or relative energy) by replacing these sites' occupation with different chemical species. Some most the most commonly used codes to build cluster expansion are the Universal Cluster Expansion Code (UNCLE) [157], Alloy Theoretic Automated Toolkit (ATAT) [100], and CLUPAN [159].

Gao et al. [72] studied TiVZrNbHfTa by adding V to the single-phase BCC forming equiatomic TiZrNbHfTa quinary system. They checked the senary system by inspecting binary and ternary phase diagrams and using enthalpy of mixing for binary compounds using the DFT. Most of the solid solution phases reported in HEAs were body-centered cubic (BCC) or face-centered cubic (FCC) structures [3,8,155]. HCP structured HEAs were limited. Few of the HCP structured HEAs reported are rare-earth-based: YGdTbDyLu [160], GdTbDyTmLu [160], YDyHoGdTb [161], or a combination of refractory and rare earth elements, i.e., ScTiYZrLaHf [162] and AlScTiZrHf [163]. Nagase et al. [164] used the concept of liquid phase separation to design the dual hexagonal closed pack (HCP) structure in TiYZrLaHf. They designed the dual HCP structure using mixing enthalpy data for the binary subsystems and phase diagrams constructed using Materials Project. They obtained Ti-Zr-Hf rich dendrite and Y-La rich inter-dendrite in the as-cast ingot. TiZrHfNbV and TiZrHfNbCr refractory alloys were fabricated using an induction melting route by Fazakas et al. [143]. It is important to note that TiZrHfNbV alloy formed a single BCC phase, whereas TiZrHfNbCr exhibited BCC as the major phase co-existing with a small amount of $NbCr_2$ and $HfCr_2$ cubic (C15)

Laves phases. The structural and mechanical properties were reported to remain unchanged up to 900 °C.

From the above reported refractory HCP and BCC HEAs Ti, Zr and Hf are common elements. Co, Cr, Mo, Nb and Ta can also be added to Ti, Zr, and Hf, HEAs for medical applications. Nagase et al. [165] developed TiZrHfCrMo and TiZrHfCoCrMo as metallic biomaterials. They claimed to have better hardness and biocompatibility of the present alloy than previously used Ti-based alloys for surgical implants. Calin et al. [166] developed TiZrHfNbSi HEA as a magnetic resonance imaging compatible metallic glass. This glassy alloy exhibited ultralow magnetic susceptibility and a superior X-ray attenuation coefficient. Huang et al. [167] prepared TiZrHf based on three refractory alloys, e.g., TiZrHfSc, TiZrHfY, and TiZrHfScY HEAs. Addition of Sc to a single HCP structured TiZrHf alloy resulted in a dual HCP structure, having improved strength and ductility. In contrast, adding Y to the TiZrHf alloy resulted in two HCP phases. The primary HCP phase is disordered with a small amount of undissolved Y (HCP2). Adding Sc and Y to TiZrHf alloy resulted in a dual HCP phase and a small amount of undissolved Y.

In the present study, we aimed at studying the phase stability of the HCP phase by adding V to previously studied TiZrHfY HEA. TiZrYHf alloy forms a single-phase HCP along with a small amount of undissolved Y. A theoretical and experimental investigation of TiVYZrHf RHEA was carried out in the present study to understand the phase evolution and stability. It may be interesting to understand the effect of V addition on the TiYZrHf HEA as the likelihood of Laves phase formation increases since the C15 type of Laves phase is very stable in Hf-V and Zr-V binary systems.

5.2.1 Phase prediction based on parametric and CALPHAD approaches

A few parameters were calculated based on the extended Hume-Rothery rules for solid solution forming. These consisted of (i) enthalpy of mixing (ΔH_{mix}^{ij}) for the binary subsystems using Miedema model (ii) weighted average of atomic size mismatch (δ) and (iii) valence electron concentration (VEC). The enthalpy values for the binary subsystems are shown in **Table 5.7**. It indicated that Ti-Zr, Hf-Ti and Hf-Zr had good mutual solubility, whereas Ti-V, V-Zr and Hf-V had significant negative enthalpy indicating the formation of intermetallic phases. Y has a highly positive enthalpy of mixing with the other elements of the groups, meaning that Y may be immiscible with other elements of the alloy. The enthalpy of mixing value for the quinary alloy (ΔH_{mix} =7 kJ mol^{-1}) was calculated by extrapolating the enthalpy of mixing of binary alloys using the regular solution model, shown in **Table 5.8**. The atomic size mismatch parameter is calculated using the formula proposed by Fang [168]. This indicated severe lattice distortion that is experienced by the parent lattice in a multicomponent system. Zhang et al. [38] proposed that for the solid solution formation in any alloy δ parameter must be ≤ 6.6. Valence electron concentration (VEC) values represent the total number of electrons present in the valence band and help in deciding the type of phases (BCC or FCC) that may form. Guo et al. [36] reported formation of FCC phase was favourable for VEC ≥ 8, whereas single-phase BCC structure was expected for VEC ≤ 6.8. For intermediate values lying in between the specified range, mixture of two phases may form (BCC+FCC).

We calculated the binary phase diagrams for the ten binary subsystems that formed on choosing five elements using Thermo-Calc. Binary alloy subsystems were computed using the SGTE solution database version 5. Analyzing **Figure 5.12** indicates that Hf-Ti, Hf-Zr and Ti-Zr had good mutual solubility and the disordered HCP phase was the equilibrium phase, whereas Hf-Ti, Ti-V and V-Zr exhibited a small miscibility

gap, resulting in a two-phase mixture. One can easily record the high miscibility gaps present in Hf-Y, Ti-Y, V-Y, and Y-Zr phase diagrams shown in **Figure 5.12**. At room temperature two-phase mixture of disordered HCP1 and HCP2 formed in Ti-Y and Y-Zr phase diagrams, while BCC_B2 and disordered HCP phases formed in Hf-Y and V-Y phase diagrams. No other Laves phase except for ZrV_2 formed in the V-Zr phase diagram could be seen.

Table 5.7: Enthalpy of mixing (in $kJ.mol^{-1}$) for all the binary sub-systems in TiVYZrHf HEA.

Elements	Ti	V	Y	Zr	Hf
Ti	-	-2	15	0	0
V	-2	-	17	-4	-2
Y	15	17	-	9	11
Zr	0	-4	9	-	0
Hf	0	-2	11	0	-

The equilibrium diagram of the chosen quinary alloy system was calculated using Thermo-Calc. **Figure 5.13** showed that above 1200 K, only the BCC_B2 phase was stable, while below 500 K, three HCP and one Laves phase were stable. The liquidus and solidus boundaries of TiVZrYHf HEA were at temperatures ~1900 K and ~1800 K, respectively. The BCC_B2 phase was the first solid phase that precipitated from the liquid phase. At ~1200 K, a disordered HCP_A3 precipitated from BCC_B2 followed by another disordered HCP_A3#2 phase at 1000 K. Due to the diffusive transformation of the BCC_B2 into HCP_A3 and HCP_A3#2, the amount of B2 phase decreased, and the disordered phase increased. At ~ 500K, all the BCC_B2 transformed into three disordered HCP and ZrV_2 (cubic Laves phase). The single point equilibrium calculation done at three temperatures are tabulated in **Table 5.9**.

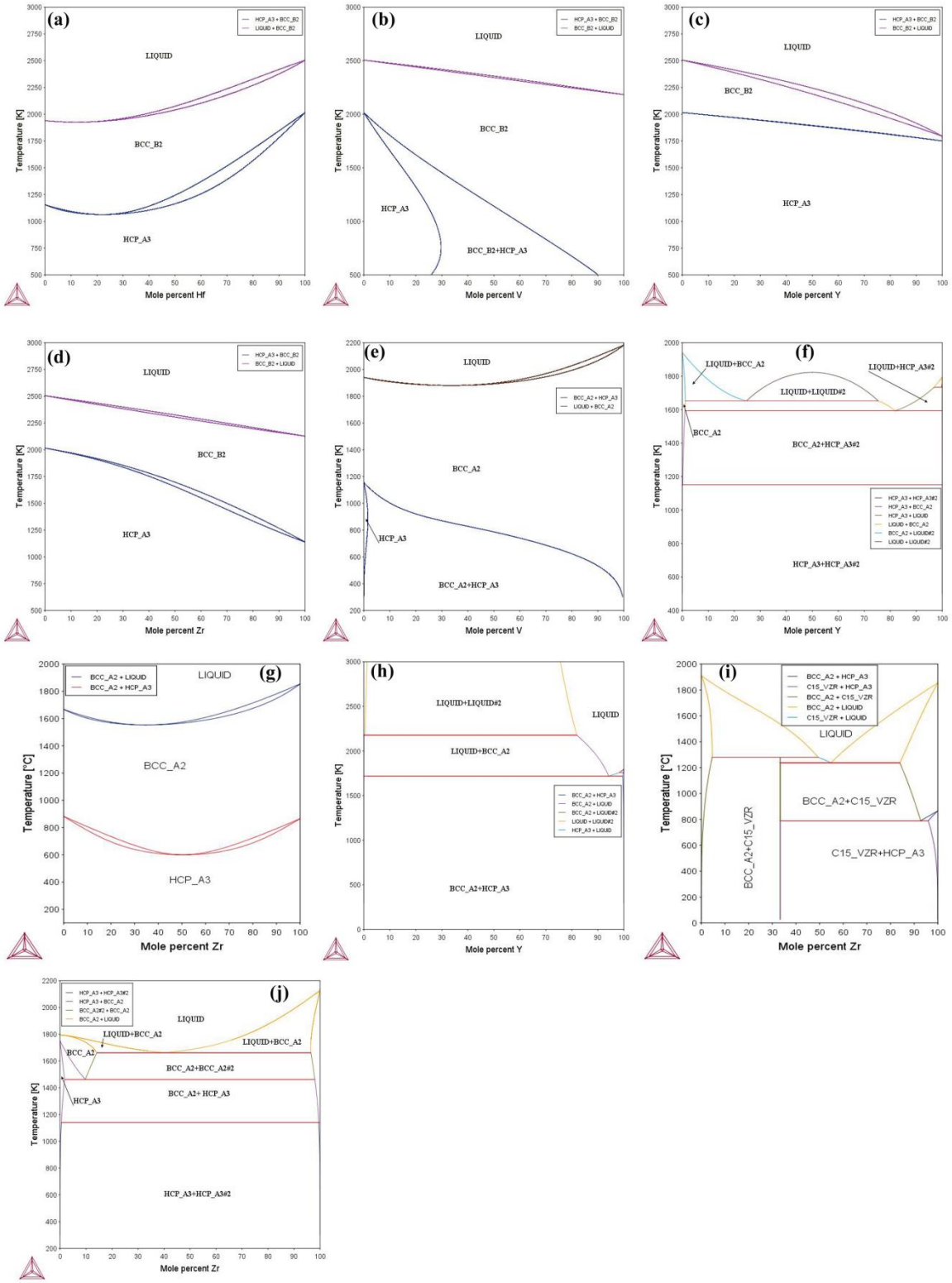

Figure 5.12: Phase diagrams of binary subsystems calculated by Thermo-Calc showing equilibrium phases. The binary phase diagrams are as follows: (a) Hf-Ti (b) Hf-V (c) Hf-Y (d) Hf-Zr (e) Ti-V (f) Ti-Y (g) Ti-Zr (h) V-Y (i) V-Zr (j) Y-Zr.

Table 5.8: Phase stability parameters calculated using the semi/empirical approaches, showing phase separation tendency in the quinary alloy system.

ΔH_{mix} (kJ.mol^{-1})	ΔS_{mix} (J.mol^{-1}K^{-1})	$\delta \times 100$ (%)	VEC
7	13.38	10.37	4

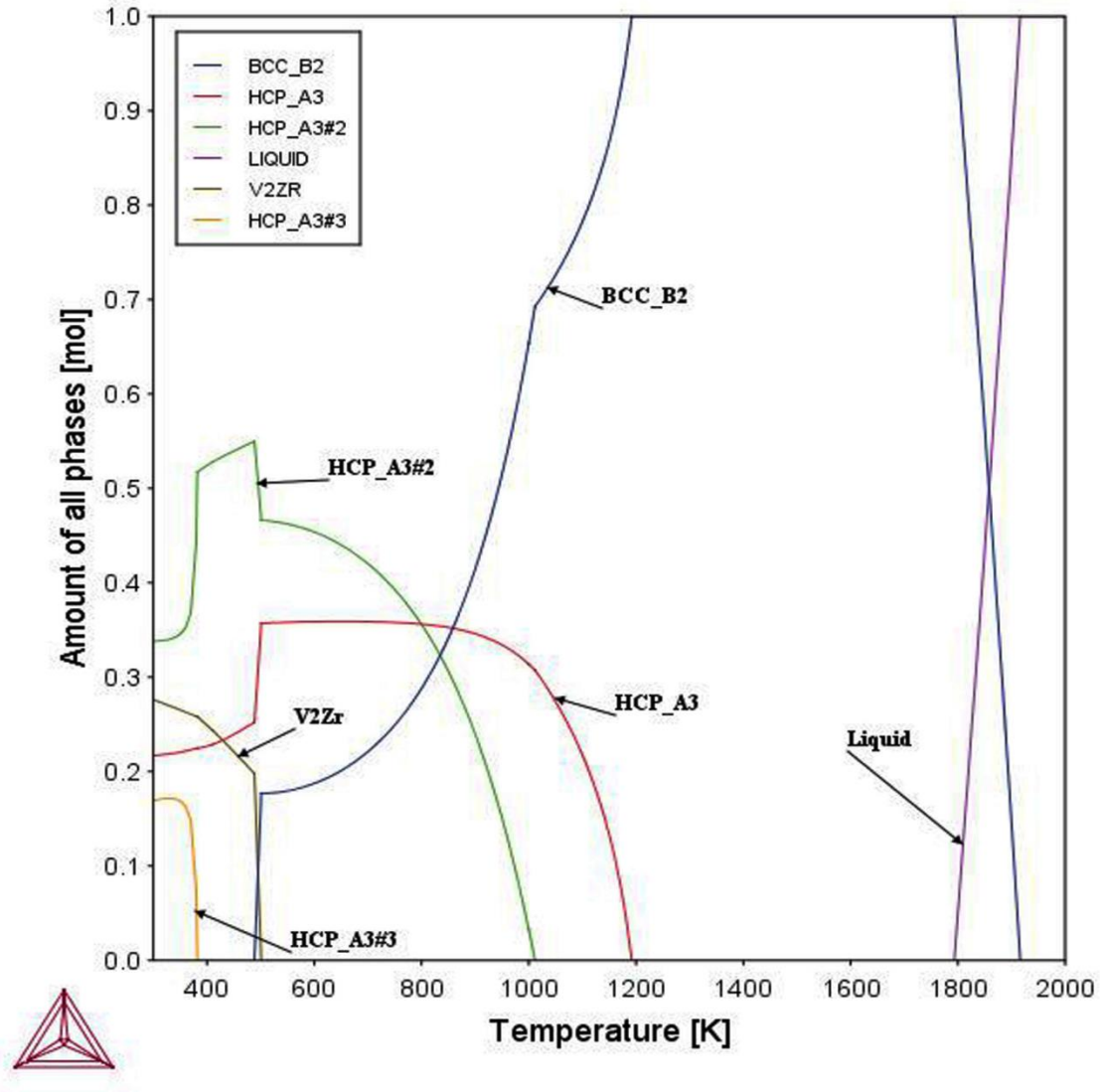

Figure 5.13: Plot of the number of equilibrium phases as a function of temperature in TiVYZrHf RHEA. The phase diagram shows a single BCC_B2 structure above 1200 K and a mixture of three disordered HCP phases and the C15 type Laves phase below 227 K.

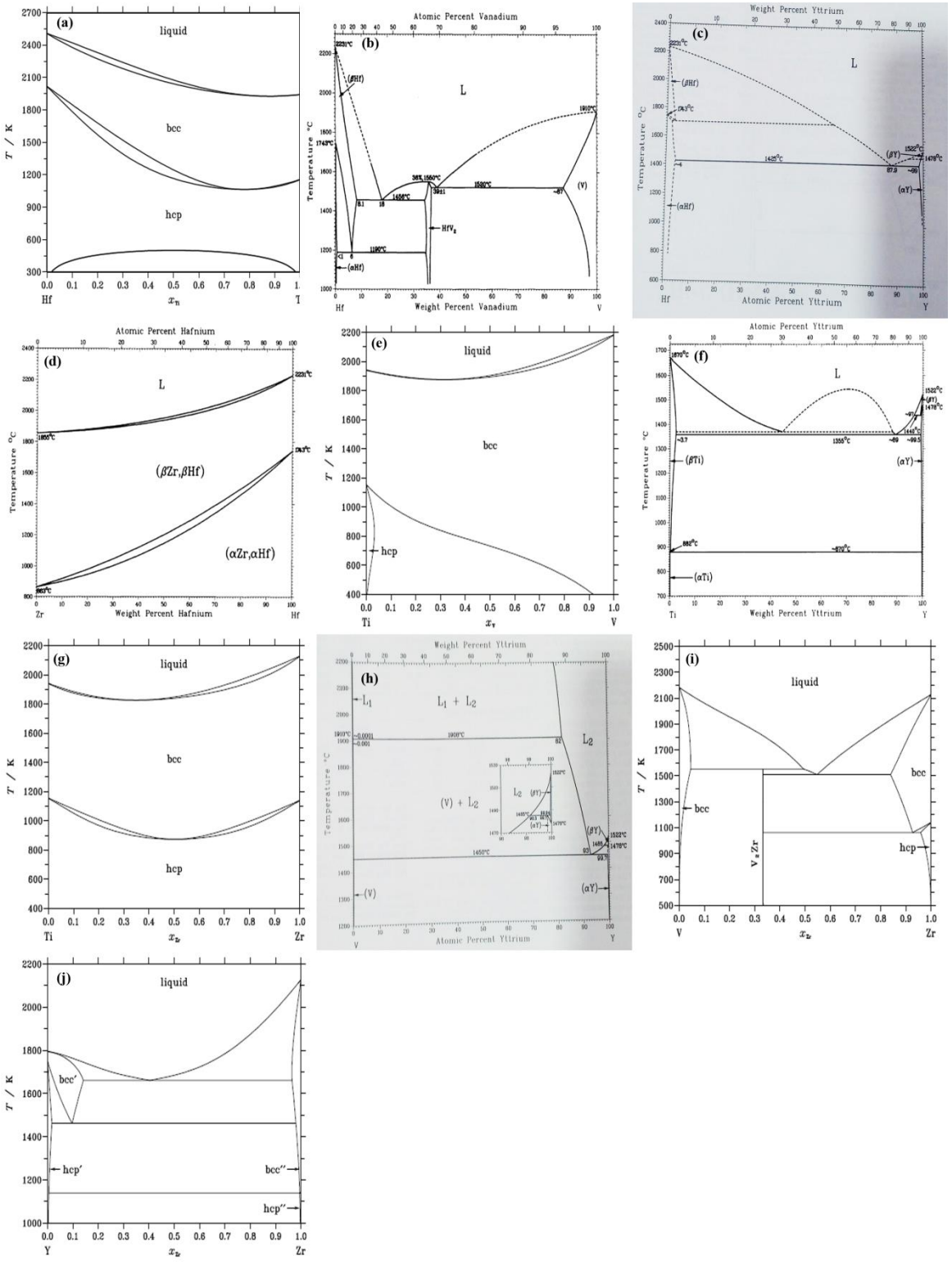

Figure 5.14: Phase diagrams of all the binary subsystems taken from the Binary alloy Phase Diagrams handbook [169] and Landolt-Bornstein database (a) Hf-Ti (b) Hf-V (c) Hf-Y (d) Hf-Zr (e) Ti-V (f) Ti-Y (g) Ti-Zr (h) V-Y (i) V-Zr (j) Y-Zr

Table 5.9: Composition of all the phases formed at 300 K, 700 K and 1100K in mole fraction estimated by single point equilibrium calculation of TiVYZrHf RHEA.

Temp (K)	Equilibrium Phase	Mole fraction	Ti	V	Y	Zr	Hf
300	HCP_A3#1	0.169	0.070	0.080	0.394	0	0.455
	HCP_A3#2	0.217	0.037	0	0	0.498	0.464
	HCP_A3#3	0.338	0.532	0.007	0.395	0	0.066
	C15_ZrV_2	0.276	0	0.667	0	0.333	0
700	HCP_A3#1	0.359	0.203	0.020	0.004	0.540	0.233
	HCP_A3#2	0.420	0.223	0.162	0.372	0.011	0.230
	BCC_B2	0.221	0.151	0.562	0.191	0.006	0.089
1100	BCC_B2	0.782	0.213	0.242	0.248	0.108	0.188
	HCP_A3#1	0.218	0.154	0.047	0.026	0.529	0.243

We have also collected phase diagrams from the Binary Alloy Phase Diagrams handbook [169], which are shown in **Figure 5.14**. It may be noted that there are considerable differences in the Hf-V and Hf-Y phase diagrams calculated using Thermo-Calc and those given in Massalski's handbook. The discrepancy in the computed binary phase diagrams of Hf-V and Hf-Y systems is due to the fact that the Thermo-Calc database used might not have been optimized for these systems.

5.2.2 Phase stability study using DFT

Phase stability study of the chosen alloy (TiVZrYHf) was studied using DFT. A 10 atom primitive cell was selected to calculate the minimum energy of formation for the quinary RHEA, as shown in **Figure 2.2**. Similarly, a 10 atom cell of HCP was selected, as shown in **Figure 2.3**. Now the arrangement of the atoms was changed, and the energy of each distinct configuration was calculated. The minimum and the maximum energy of

formation from the calculated list is shown in **Table 5.10**. which displays the critical point of miscibility gap as calculated by the regular solution model using the formula [170]

$$T_c(K) = \frac{\Delta H_{mix}}{2R} \tag{5.1}$$

R is the gas constant, and K represents the temperature obtained in kelvin (K). The formation energy of a few possible intermetallic phases is also calculated and reported in **Table 5.11**. The two intermetallics HfV_2 and ZrV_2 were taken from the binary phase diagrams, and the formation of energy for these phases was calculated. Having very good mutual solubility between Hf and Zr, we also checked the possibility of forming the ternary Laves phase. These ordered phases formation energy has very minute differences, showing the (Hf, Zr)V_2 having minimum energy. Thus we have considered the formation of the ternary Laves phase in the alloy and indexed it in the XRD pattern.

Table 5.10: Energy of formation for 10 atoms primitive cell and HCP cell are calculated, and the maximum and minimum values are tabulated. As the formation energy is significantly positive, we have calculated the miscibility gap's critical temperature using a regular solution model.

Phases	**BCC**		**HCP**	
	Minimum	**Maximum**	**Minimum**	**Maximum**
TiVYZrHf (kJ.mol^{-1})	30.973	42.380	23.845	39.644
Critical point (K)	1863	2549	1434	2384

5.2.3 Characterization of the annealed sample.

The as-cast sample was annealed for 2 h, and the furnace cooled to obtain the equilibrium phases formed in the chosen alloy system. The XRD of the annealed sample was done to predict the crystal structure of the evolved phases, as shown in **Figure 5.15.** From the figure, we were able to recognize multiphase alloy containing three disordered

and one ordered phases. The three disordered phases were HCP1(a= 3.18 ± 0.02 Å, c/a=1.58), HCP2 (a= 3.67 ± 0.02 Å, c/a= 1.55), and BCC (a= 3.16 ± 0.02 Å), while the ordered one was (Hf, Zr)V_2 (C15 type Laves phase, a= 7.41 ± 0.02 Å).

Table 5.11: Formation energy (kJ.mol^{-1}) of possible intermetallics taken from phase diagrams are calculated using DFT.

Phases	**HfV_2**	**ZrV_2**	**(Hf, Zr)V_2**
Formation Energy (kJ.mol^{-1})	-11.897	-10.777	-11.391

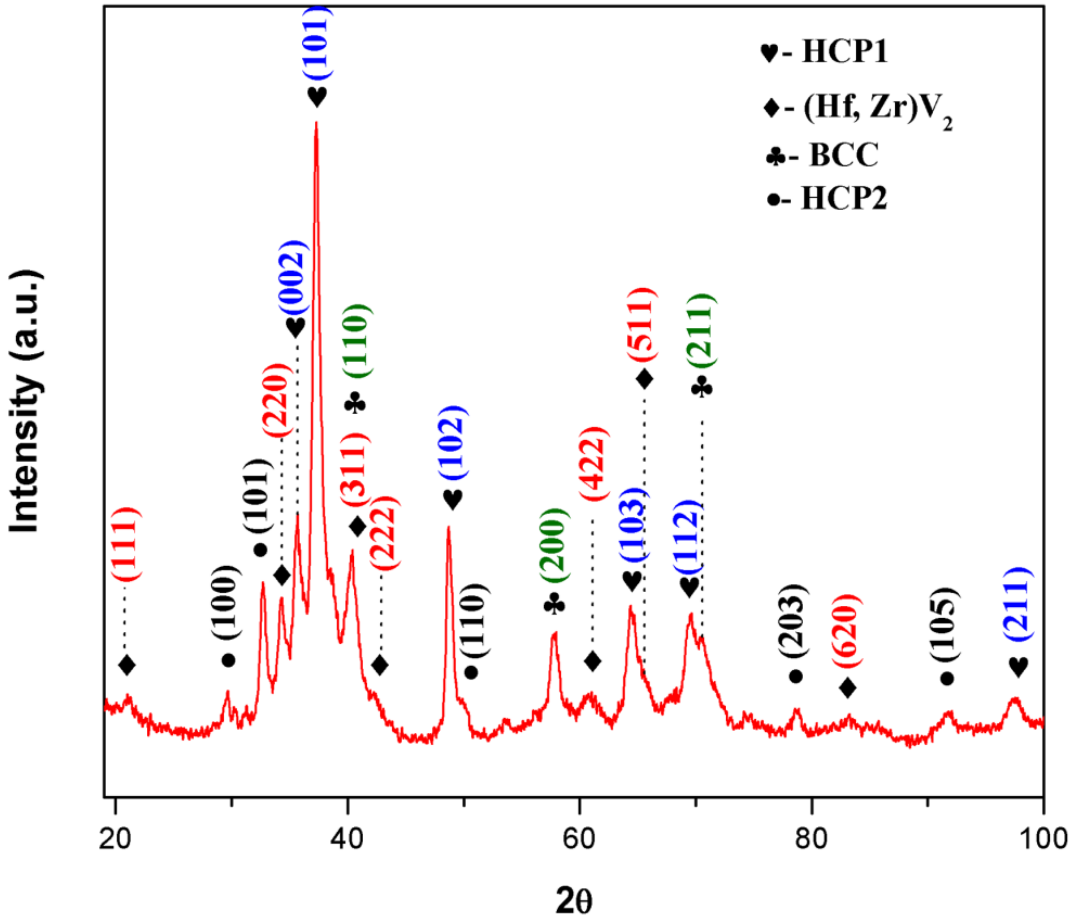

Figure 5.15: Phases evolved after annealing the as-cast sample for 7 h encapsulated in an argon-filled quartz tube at 900 °C.

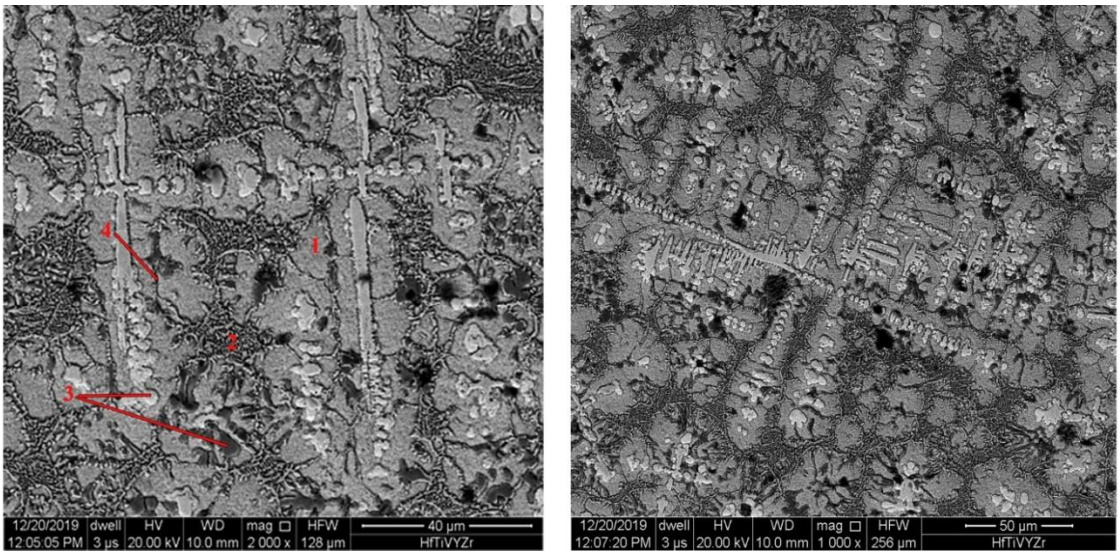

Figure 5.16: SEM micrographs of an annealed sample. The area marked 1 represents the primary phase, while the area marked 2 illustrates the eutectic kind of lamellar phases formed. The area pointed as 3 represents the phase that solidified the last forming droplet kind of structure, while the thin boundary marked as 4 represents the liquid phase between grain boundaries that solidify after the formation of the primary phase.

The morphology and microstructure of the annealed sample were examined by SEM, as shown in **Figure 5.16**. From the figure, we can clearly identify three types of microstructure, i.e., the major phase marked as 1, the eutectic kind of lamellar phase marked as 2, and the droplet structure marked as 3. The intergranular boundary of the major phase contains a thin solidified liquid phase marked as 4. In order to examine the overall composition of the bulk sample full area scan was done to obtain the average composition of the bulk phase, as shown in **Figure 5.17**. All the elements were evenly distributed except yttrium. The spot analysis of the two varying microstructures was examined, as shown in **Figure 5.18** and **5.19. Figure 5.18** deals with the composition of the primary phase, showing Hf and Zr rich phase with some quantity of Ti alloyed in it. Whereas **Figure 5.19** deals with the lamellar microstructure formed in the alloy, it contains all the elements except Y.

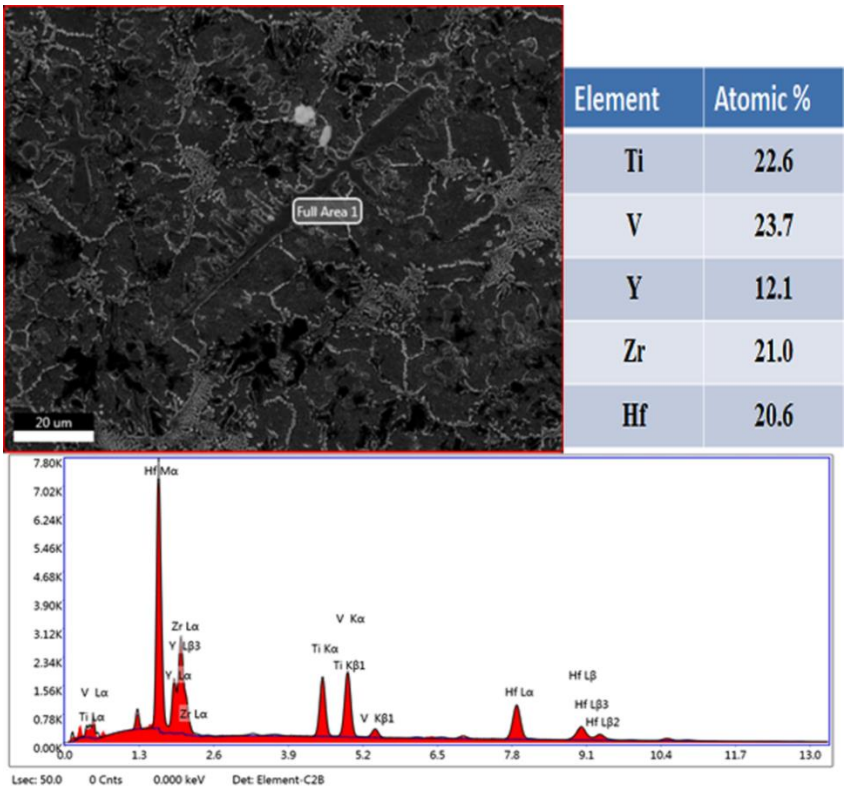

Element	Atomic %
Ti	22.6
V	23.7
Y	12.1
Zr	21.0
Hf	20.6

Figure 5.17: SEM-EDAX of the annealed sample. A full area scan is done to obtain the average composition of the bulk sample.

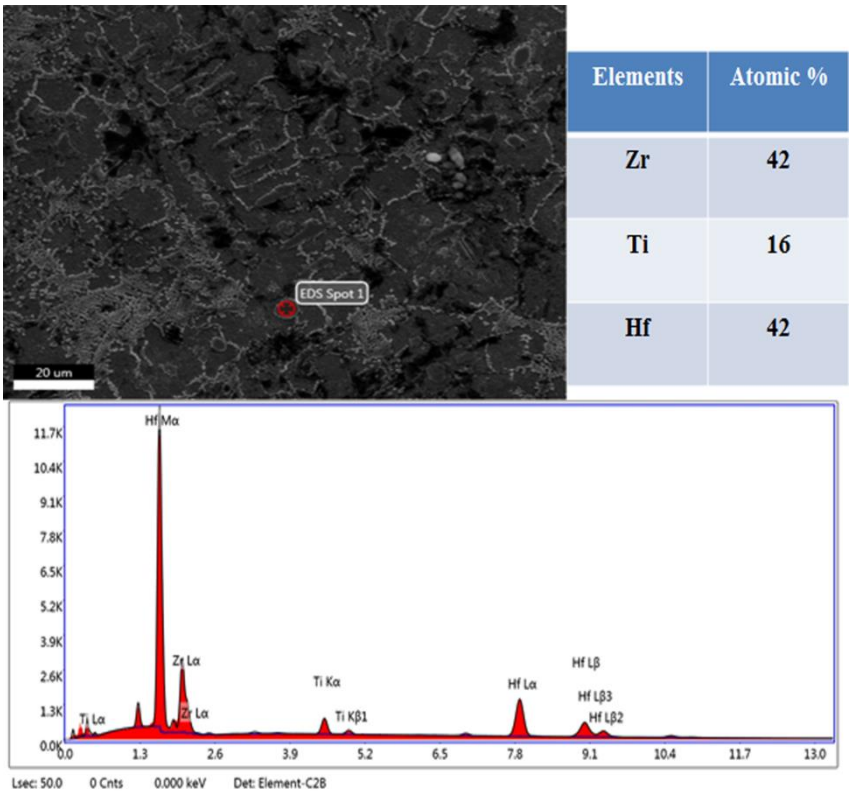

Elements	Atomic %
Zr	42
Ti	16
Hf	42

Figure 5.18: SEM-EDS of the spot on the major phase of the annealed sample.

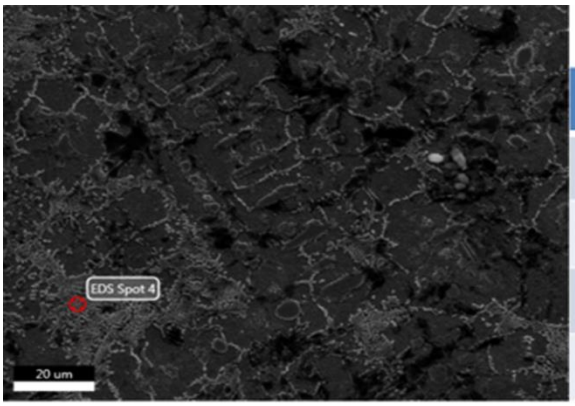

Element	Atomic %
Ti	32.5
V	23.2
Zr	24.4
Hf	19.8

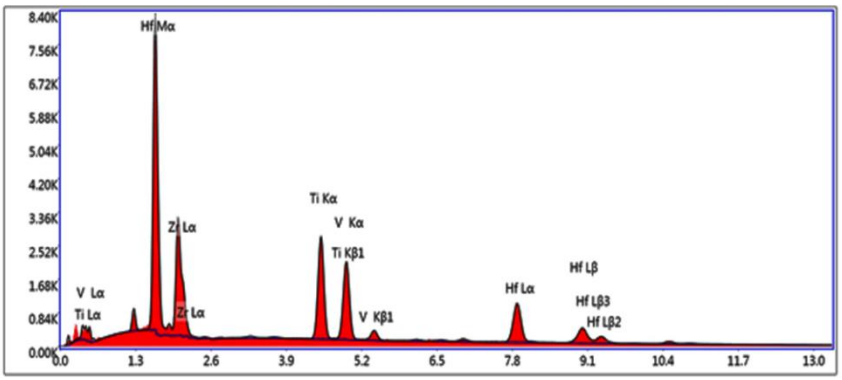

Figure 5.19: SEM-EDS analysis of the lamellar microstructure in the annealed sample showing the presence of all the elements except Y.

5.2.4 Discussion

Parametric calculations were done to understand the initial behavior of the chosen alloy. The enthalpy of mixing plays a dominant role in investigating the effect of the thermodynamics on the constituent elements' behavior in the alloy. The enthalpy of mixing for the binary subsystems were calculated using Miedema's model [45]. The mixing of enthalpy values is tabulated in **Table 5.7**. On investigating the values, it can be seen that all the elements have good mutual solubility among themselves except with yttrium. The V-Zr and Hf-Zr binary systems have significant negative enthalpy values, indicating the chances of forming intermetallic phases. The enthalpy of mixing values of the chosen alloy was calculated using extrapolation of binary values to a quinary system using a regular solution model [171]. The calculated enthalpy of mixing value (7 $kJ.mol^{-1}$) is shown in **Table 5.8**. The atomic size mismatch plays a critical role in the stability of

the system. The weighted average of the atomic size mismatch as tabulated in **Table 5.8** is higher than the desired value, this may de-stabilize the lattice, and multiphase microstructure may form. The solid solution forming criteria as proposed by Zhang et al. [38] and discussed in the previous chapter was matched with the calculated values of ΔH_{mix} (7 kJ.mol^{-1}), ΔS_{mix} (13.38 J.mol^{-1}.K^{-1}), δ (10.37 %), and VEC (4). In comparison, we found that ΔH_{mix} and δ being out of the given range, resulted in the multiphase microstructure.

Examining the binary phase diagrams calculated using Thermo-Calc (**Figure 5.12**) and taken from the Binary Alloy Phase Diagrams book (**Figure 5.14**), we found similar results as predicted by the Miedema method. From Phase diagrams, it can be pointed out that Hf-Ti, Ti-Zr, and Hf-Zr show isomorphous phase diagrams, while Hf-V and V-Zr show ordered intermetallics (C15 type Laves phase) at room temperature. The Ti-V phase diagram has some tendency of phase separation. Simultaneously, the binary phase diagrams of the Y with other constituent elements have a high miscibility gap (up to liquid phase).

The XRD analysis of the annealed sample (**Figure 5.15**) shows four types of phase formation. The HCP1 (a= 3.18 ± 0.02 Å, c= 5.02 ± 0.02 Å) being a major phase. The SEM-EDS mapping shows that the primary phase is rich in equiatomic type Hf-Zr solid solution with a small amount of Ti. The second type of morphology is shown in **Figure 5.16,** representing a eutectic kind of reaction (lamellar structure). The SEM-EDS compositional analysis illustrates the presence of all elements except Y (**Figure 5.19**). We may predict that the lamellar portion consists of (Hf, Zr)V_2 and Ti-V phase on comparing the XRD and SEM-EDS results. The fourth HCP2 phase is Y rich phase, which solidified, at last forming a droplet-like microstructure as shown in SEM micrographs.

The formation of a multiphase matrix was also supported by DFT calculations shown in **Table 5.10**. The critical point of the miscibility gap calculated using DFT calculation and the regular solution model is ~1434 (1161 °C), while the prediction of CALPHAD show precipitation of the new phase at ~ 1000 °C. The small discrepancies may be due to the unavailability of the assessed data of three binary systems (Hf-Y, Ti-Y, and V-Y) in the SSOL5 database of Thermo-Calc. Having the highly positive enthalpy values indicate phase separation and formation of binary and ternary phases. Thus the phase stability of binary phases was examined by calculating their formation energy (**Table 5.11)**. The calculation favors the formation of the ternary Laves phase (Cubic type). The lattice parameter of all elements was calculated using DFT (for FCC, BCC and HCP phases). The composition of the primary phase is examined through SEM-EDS (TiZrHf). Applying the rule of a mixture using composition from SEM-EDS and the lattice parameter from DFT, we predicted the lattice parameter of the TiZrHf disordered phase (3.16 Å). Assuming the BCC phase as equiatomic, we have predicted the lattice parameter to be equal to 3.13 Å. The predicted lattice parameters were in accordance with the calculated parameters from XRD.

Table 5.12: Prediction of lattice parameter based on the rule of mixture. The lattice parameter of TiZrHf is predicted based on the composition of the major phase obtained from SEM-EDS (Figure 5.18), while that of TiV is assumed to be the equiatomic phase.

Elements	**BCC**	**FCC**	**HCP**		**Lattice parameter (Å)(TiZrHf)**	**Lattice parameter (Å)(TiV)**
	a (Å)	**a (Å)**	**a (Å)**	**c/a**		
Ti	3.24	4.11	2.94	1.58	3.16	3.13
V	3.02	3.81	2.95	1.63		
Y	3.49	5.05	3.65	1.55		
Zr	3.57	4.52	3.23	1.59		
Hf	3.08	4.44	3.19	1.58		

5.3 Conlusions

Following conclusions can be drawn from the section 5.1 and 5.2

5.3.1 TiVZrMoW

1. Enthalpy of mixing of this TiVZrMoW high entropy alloy calculated using Miedema's models, (ΔH_{mix}^{Mied} ~ -4.25 kJ.mol^{-1}), lies within the range of the solid solution formation ($-10 \leq \Delta H_{mix} \leq 5$ kJ.mol^{-1}). VEC for the alloy observed to be 5, can favour the formation of a single BCC phase. However, size mismatch factor, δ (7.17 %), being on the higher range, could be held responsible for de-stabilize the lattice to form a multi-phase structure. Hence, the experimental observation of multiphase is in agreement with the prediction by the theoretical approaches.
2. Enthalpy of mixing of the alloy for BCC was calculated using extrapolation of the enthalpy value of the disordered 8 atom SQS of binary subsystems and found to be 4.25 kJ.mol^{-1}, which was lower than that of the FCC and HCP structures. Thus the BCC could be more stable than other structures, but having a possibility of miscibility gap at a lower temperature leading to multiple structures.
3. As per the prediction of the CALPHAD approach, three ordered BCC phases along with two Laves phases were found to be stable at ~500 °C, whereas only two BCC phases are stable above ~ 600 °C. However, the three BCC phases as predicted were not found in this experimental observation. This requires further investigation.

4. The as-cast alloy showed the presence of two BCC phases i.e., major bcc1 (3.17 ± 0.02 Å) being Mo and W rich, and minor bcc2 (3.65 ± 0.02 Å) being Ti and Zr rich along with C15 type ternary Zr(Mo, W)$_2$ Laves phase (7.58 ± 0.02 Å).
5. The DSC analysis of the as-cast sample showed two endothermic peaks of solid-solid transformation up to 620 °C. However, the alloy does not show any transformation in the temperature range, 620 – 1000 °C.
6. The annealed sample (900 °C) exhibited that two BCC phases present in the as-cast sample were transformed into the ordered B2 structures. The SEM-EDS mapping of the annealed sample showed that the primary major B2 phase contained W and Mo predominantly, while the other minor B2 phase contained Ti and Zr.

5.3.2 TiVZrYHf

1. Enthalpy of mixing of TiVYZrHf high entropy alloy was calculated using Miedema model (ΔH_{mix} = 7 kJ.mol^{-1}) found to be close to the proposed range favouring the formation of single-phase solid solution ($-10 \leq \Delta H_{mix} \leq 7 kJ.mol^{-1}$). However, the size mismatch factor δ (10.37 %) was on the higher side favouring the formation of the multiphase structures. Similarly, the enthalpy of mixing calculated using DFT (ΔH_{mix}^{DFT} = 23.845 kJ.mol^{-1}) with the minimum value for the HCP phase was obtained.
2. As per the prediction of the CALPHAD approach, three disordered HCP and one Laves phase (ZrV_2) were found to be stable at room temperature, whereas the BCC_B2 phase was identified to be stable above 1000 °C.
3. The annealed sample showed the presence of two disordered HCP1(a = 3.18 ± 0.02 Å, c/a = 1.58) and HCP2 (a = 3.67 ± 0.02 Å, c/a = 1.55), along with BCC

(a = 3.16 ± 0.02 Å) and the ordered (Hf, Zr)V_2 phase (C15 type Laves phase, a = 7.41 ± 0.02 Å) supporting the theoretical prediction. The SEM-EDS mapping of the annealed sample revealed that the primary major HCP1 phase containing predominantly Hf and Zr along with some amount of Ti.

4. Applying the rule of a mixture using composition from SEM-EDS and the lattice parameter from DFT, we have predicted the lattice parameter of the TiZrHf disordered phase (3.16 Å). Assuming the BCC phase as equiatomic, we have predicted the lattice parameter to be equal to 3.13 Å. The predicted lattice parameters were in accordance with the calculated parameters from XRD being 3.18 Å and 3.16 Å, respectively.